LEVEL

HORIZONTAL BUOYANCY EFFECTS ON THE PRESSURE
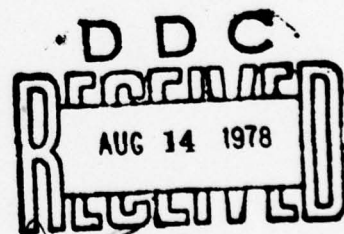DISTRIBUTION OF AN AXISYMMETRIC BODY OPERATING
IN A CYLINDRICAL DUCT

Lauchle, G. C.

The Pennsylvania State University
Institute for Science and Engineering
APPLIED RESEARCH LABORATORY
Post Office Box 30
State College, Pa. 16801

DDC
RECEIVED
AUG 14 1978
A

NAVY DEPARTMENT

NAVAL SEA SYSTEMS COMMAND

78 08 04 031

SECURITY CLASSIFICATION OF THIS PAGE (When Data Entered)

REPORT DOCUMENTATION PAGE		READ INSTRUCTIONS BEFORE COMPLETING FORM
1. REPORT NUMBER TM-78-170	2. GOVT ACCESSION NO.	3. RECIPIENT'S CATALOG NUMBER
4. TITLE (and Subtitle) HORIZONTAL BUOYANCY EFFECTS ON THE PRESSURE DISTRIBUTION OF AN AXISYMMETRIC BODY OPERATING IN A CYLINDRICAL DUCT (U)		5. TYPE OF REPORT & PERIOD COVERED Technical Memorandum
		6. PERFORMING ORG. REPORT NUMBER
7. AUTHOR(s) G. C. Lauchle		8. CONTRACT OR GRANT NUMBER(s) N00017-73-C-1418
9. PERFORMING ORGANIZATION NAME AND ADDRESS Applied Research Laboratory P. O. Box 30 State College, PA 16801		10. PROGRAM ELEMENT, PROJECT, TASK AREA & WORK UNIT NUMBERS
11. CONTROLLING OFFICE NAME AND ADDRESS Naval Sea Systems Command Washington, DC 20362		12. REPORT DATE June 1, 1978
		13. NUMBER OF PAGES 35
14. MONITORING AGENCY NAME & ADDRESS(if different from Controlling Office)		15. SECURITY CLASS. (of this report) UNCLASSIFIED
		15a. DECLASSIFICATION/DOWNGRADING SCHEDULE

16. DISTRIBUTION STATEMENT (of this Report)

Approved for Public Release. Distribution Unlimited
Per NAVSEA - July 24, 1978.

17. DISTRIBUTION STATEMENT (of the abstract entered in Block 20, if different from Report)

18. SUPPLEMENTARY NOTES

19. KEY WORDS (Continue on reverse side if necessary and identify by block number)

hydrodynamics water tunnel
pressure
buoyancy
wall interference

20. ABSTRACT (Continue on reverse side if necessary and identify by block number)

(U) It is well known that the static pressure coefficient values obtained from tests of axisymmetric bodies in, for example, a large water tunnel indicate the existence of tunnel wall interference. This interference is due to blockage experienced by the body operating within the boundaries of the test section walls, and to the skin friction on both the tunnel walls and the surface of the body, which in turn causes finite thickness boundary layers to develop. These factors result in a decrease in static pressure

DD FORM 1473 1 JAN 73 EDITION OF 1 NOV 65 IS OBSOLETE

along the test section which leads to a spurious horizontal buoyancy on the body. These interferences become more important as the size of the body increases relative to the fixed dimensions of the test section. Potential flow calculations can only account for solid blockage effects. A control volume analysis has thus been carried out from which pressure coefficient correction terms due to horizontal buoyancy have been obtained. They may be directly applied to any inviscid pressure distribution calculated for any given body operating in a given tunnel. These correction factors are computed for a large, streamlined body operating over a range of velocities, in The Pennsylvania State University, Garfield Thomas 1.22-m. diameter Water Tunnel. They are applied to a theoretically-determined potential flow, in-tunnel body pressure distribution to obtain the viscous flow pressure distributions which are compared to those determined experimentally. The agreement between theory and experiment is shown to be very good over all speeds considered. Traditional methods of accounting for horizontal buoyancy which are obtained from measurements of the longitudinal static pressure gradient in a clear tunnel, are applicable only to small bodies. The present method permits one to treat relatively large bodies which have a much stronger interaction with the tunnel walls.

Subject: Horizontal Buoyancy Effects on the Pressure Distribution of
           an Axisymmetric Body Operating in a Cylindrical Duct

References: See page 26

Abstract: It is well known that the static pressure coefficient values
           obtained from tests of axisymmetric bodies in, for example, a
           large water tunnel indicate the existence of tunnel wall inter-
           ference. This interference is due to blockage experienced by
           the body operating within the boundaries of the test section
           walls, and to the skin friction on both the tunnel walls and
           the surface of the body, which in turn causes finite thickness
           boundary layers to develop. These factors result in a decrease
           in static pressure along the test section which leads to a
           spurious horizontal buoyancy on the body. These interferences
           become more important as the size of the body increases relative
           to the fixed dimensions of the test section. Potential flow
           calculations can only account for solid blockage effects. A
           control volume analysis has thus been carried out from which
           pressure coefficient correction terms due to horizontal buoyancy
           have been obtained. They may be directly applied to any inviscid
           pressure distribution calculated for any given body operating in a
           given tunnel. These correction factors are computed for a large,
           streamlined body operating over a range of velocities in The
           Pennsylvania State University, Garfield Thomas 1.22-m. diameter
           Water Tunnel. They are applied to a theoretically-determined
           potential flow, in-tunnel body pressure distribution to obtain
           the viscous flow pressure distributions which are compared to
           those determined experimentally. The agreement between theory
           and experiment is shown to be very good over all speeds considered.

Traditional methods of accounting for horizontal buoyancy which are obtained from measurements of the longitudinal static pressure gradient in a clear tunnel, are applicable only to small bodies. The present method permits one to treat relatively large bodies which have a much stronger interaction with the tunnel walls.

Table of Contents

List of Figures

List of Tables

Nomenclature

A	the blocked area between the body and duct wall
A_e	the effective area between the body and duct wall including displacement thickness effect
A_o	area of duct
a	numerical constant in Eq. (46)
B_i	the continuity integral, Eq.'s (40) and (41)
C_o	numerical constant in Eq. (46)
Cp	pressure coefficient
ΔCp	pressure coefficient correction
ΔCp_i	components of ΔCp (i = 1, 2, ...)
ΔCp_{11}	ΔCp_1 for laminar-body flow
ΔCp_{12}	ΔCp_1 for turbulent-body flow
D_{max}	maximum diameter of the body
d_o	distance from nose of body to geometrical beginning of the water tunnel test section
F_i	fluid forces (i = 1, 2, ...)
I_i	the momentum integral, Eq.'s (37) and (38)
K_n	body fineness ratio (ℓ_n/D_{max})
k	numerical constant in Eq. (46)
L	total body length
ℓ	duct length used in potential flow calculation
ℓ_o	distance from nose of body to point on duct wall where turbulent boundary layer begins
ℓ_n	distance from body nose to D_{max}
P_o	free-stream static pressure

p	local fluid pressure
P_b	pressure exerted by the body on the fluid
P_b'	"displaced-body" pressure exerted by the body on the fluid
R_L	radius of curvature of the body tailcone
Re_L	body-length Reynolds number
r	radius coordinate
s	arc length coordinate
s_t	transition arc length
U_∞	free-stream velocity in duct far upstream of body
u	local fluid velocity
u_i	velocity profile for body ($i = 1$, laminar; $i = 2$, turbulent)
u_o	reference velocity in potential flow computation
u_r	numerical rake output far upstream of body (U_∞/u_o)
u_{rp}	numerical rake output near the body at, for example, a pitot probe location
x	axial coordinate where origin is ℓ_o upstream from nose of the body
$\bar{x}$	body axial coordinate ($x - \ell_o$)
$\hat{x}$	non-dimensional body axial coordinate ($\bar{x}/\ell_n$)
x'	dummy variable of integration
$\hat{y}$	non-dimensional body radius ($r_b/D_{max}/2$)
δ	boundary-layer thickness
δ_i	body boundary-layer thickness ($i = 1$, laminar; $i = 2$, turbulent)
δ^*	boundary-layer displacement thickness
ϵ_L	the expression given by Eq. (47)
υ	kinematic viscosity

ρ   fluid mass density

τ   wall shear stress

φ   angle formed between tangent line of body and the x-axis

Special Subscripts

b   refers to body

E   refers to experimental

I   refers to inviscid

m   refers to measured

V   refers to viscous

w   refers to duct wall

INTRODUCTION

The investigation of flows about bodies of revolution in cylindrical ducts is of general interest to those concerned with turbomachinery, wind tunnel, and water tunnel testing, to note a few. There have been several methods proposed for the determination of the potential flow about bodies operated within ducts of both constant and non-uniform cross section [1-5]. These methods allow for blockage effects due to the duct (or test section) walls to be accounted for. However, these methods do not allow for viscous effects that occur on the body and tunnel walls. Viscosity gives rise to skin friction on all surfaces in contact with the flowing fluid; which, in turn gives rise to boundary layer growth. The displacement thickness varies from the beginning of boundary layer growth to distant points far downstream, effectively changing the cross-sectional areas of both the body and the duct. This added constriction of the flow and the skin friction creates a second type of blockage characterized by a static pressure drop from the beginning of boundary layer growth to any arbitrary point downstream. This net change in static pressure may be interpreted in the form of a force in the horizontal direction (assuming the tunnel test section is horizontal) which is the so-called "horizontal buoyancy."

In many applications, it is necessary to know as precisely as possible, the pressure distribution on a particular body operating in a given tunnel test section. Because of horizontal buoyancy effects, a typical inviscid flow calculation will not yield totally accurate results for relatively large diameter bodies (relative to the diameter of the test section). This statement may be verified through a direct comparison of experimentally determined pressure distributions with a potential flow prediction. Figure 1 shows such a comparison. The axisymmetric

body here is 3.05-m. long and has a maximum diameter of 32.39-cm. The

pressure coefficient data were obtained on this body while it operated in

the Garfield Thomas 48-inch (1.22-m.) diameter Water Tunnel lcated at the Applied

Research Laboratory of The Pennsylvania State University. A description of

the experiments will be presented in a later section. The potential flow

calculation shown in Figure 1 was performed using the Douglas-Neumann code

[1,2]. The solid blockage due to the 1.22-m. diameter test section is included

in this computation. The experimental pressure coefficients are seen to be

lower than those predicted at a given point on the body and are velocity-

dependent. This discrepancy is due to horizontal buoyancy.

Measurements of body pressure distributions are not economically practical

in all cases. The next best alternative, therefore is to approach analytically

the problem of horizontal buoyancy. This report presents such an analysis, where

correction terms are derived that may be applied to the results of a given

potential flow calculation. As examples of the analysis, we include calcula-

tions for the body of Figure 1 and compare them with the experimentally

determined data. Although the analysis given here is for axisymmetric bodies

operating in cylindrical test sections of constant radius, it is quite general

so that its adaptation to other configurations (variable radius test sections,

for example) would seem straightforward.

<div align="center">ANALYSIS</div>

Potential Flow Considerations

The potential flow pressure distribution on an arbitrarily- shaped axisymmetric body

operating within the confines of a cylindrical duct of circular cross section may be

calculated using the Douglas- Neumann computer code [1,2], among others [3-5].

A typical computation with the Douglas-Neumann code might use the modeling shown in Figure 2(a). Because of the limited core size on our digital computers, the length of the duct (which is described by discrete points) must be finite when using this method. If the duct is assumed to extend from $\bar{x} = -\ell$ to $\bar{x} = \ell + L$, where L is the body length, then the resulting pressure coefficient values on the body (Cp) are normalized to an unspecified reference velocity, u_o. We know, however, that in the limit $\ell \to \infty$, $u_o \to U_\infty$ (U_∞ is the true velocity at infinity). Consequently, in conjunction with our computation of the potential flow about the body, we also determine $u_r \equiv U_\infty/u_o$ at $\bar{x} = -\ell$, where ℓ is assumed much larger than L. Knowing u_r, the calculated pressure coefficient values may then be corrected to the reference velocity U_∞ by a simple computation:

$$Cp_I = 1 - \left(\frac{u_I}{u_o}\right)^2 \left(\frac{u_o}{U_\infty}\right)^2$$

$$= 1 - (1 - Cp)/u_r^2 \qquad , \qquad (1)$$

where Cp_I represents the potential flow pressure coefficient on a body operating in a cylindrical tube of infinite extent. Equation (1) is most useful to use when a number of pressure distributions are to be calculated for a family of bodies and compared; it assures us of a consistent reference velocity.

By defining a control volume from Figure 2(a) to extend from $\bar{x} = -\infty$ to an arbitrary $\bar{x}$ on the body, the continuity equation may be written as

$$A_o U_\infty = A u_I \qquad , \qquad (2)$$

where

$$A_o = \pi r_w^2 \qquad , \qquad (3)$$

$$A = \pi (r_w^2 - r_b^2) \qquad , \qquad (4)$$

with r_w and r_b being the tunnel wall and body radii, respectively. We may also write the momentum flux equation:

$$\rho u_I^2 A - \rho U_\infty^2 A_o = F_1 + F_2 + F_3 \quad , \tag{5}$$

where ρ is the density of the fluid, and the F_i's ($i = 1, 2, 3$) are the forces acting on the control volume. Assuming positive forces to act in the positive x-direction, we have:

$$F_1 = P_o A_o \tag{6}$$

and

$$F_2 = -p_I A \quad , \tag{7}$$

where P_o is the free-stream static pressure, and p_I is the potential pressure that occurs in the fluid at any arbitrary location within the control volume. The third force, F_3 is due to the pressure exerted by the body in the x-direction. It depends therefore on the pressure distribution of the body, $p_b(\bar{x})$. The differential form of this force may be written as

$$dF_3 = - p_b \sin\phi \, dA_b \quad , \tag{8}$$

where ϕ is the angle between the tangent line of the body at point $\bar{x}$ and the $\bar{x}$-axis, and

$$dA_b = 2\pi r_b \, ds = 2\pi r_b \, d\bar{x}/\cos\phi \quad , \tag{9}$$

where s is the arc-length coordinate. We can integrate dF_3 along the body and get

$$F_3 = -2\pi \int_o^{\bar{x}} p_b r_b \tan\phi \, dx' \quad , \tag{10}$$

where x' is a dummy variable of integration.

We may now solve Eq. (5) for p_I (contained in F_2) and use Eq. (2) to obtain:

$$p_I = P_o \frac{A_o}{A} - \rho U_\infty^2 \frac{A_o^2}{A^2} + \rho U_\infty^2 \frac{A_o}{A} - \frac{2\pi}{A} \int_o^{\bar{x}} p_b r_b \tan\phi \, dx' \quad . \tag{11}$$

This equation describes the inviscid pressure that occurs in the fluid at location $\bar{x}$ ($0 \leq \bar{x} \leq L$). We will now derive the corresponding equation for this pressure when viscous effects are included.

Viscous Flow Considerations

Viscosity gives rise to wall shear stress and boundary layer development on both the body and the tunnel wall. A new control volume must be considered which is shown in Figure 2(b). We choose the beginning of this control volume to be a distance ℓ_o upstream of the forward stagnation point of the body, where the new axial coordinate $x = \bar{x} + \ell_o = 0$. This origin is judiciously selected to be the point where a turbulent boundary layer begins to form on the tunnel wall. We will further assume that ℓ_o is large enough relative to the body length such that the velocity is uniform across the duct at $x = 0$. Without any loss of generality, we call this velocity U_∞.

The general form of the continuity equation for the control volume of Figure 2(b) is

$$A_o U_\infty = 2\pi \int_{r_b}^{r_w} u r \, dr \qquad , \qquad (12)$$

where u is the non-uniform velocity profile between the body and tunnel wall. In like manner, we can write the change in momentum flux as

$$2\pi \rho \int_{r_b}^{r_w} u^2 r \, dr - \rho U_\infty^2 A_o = \sum_{i=4}^{8} F_i \qquad , \qquad (13)$$

where

$$F_4 = P_o A_o \quad , \tag{14}$$

$$F_5 = -P_V A \quad , \tag{15}$$

$$F_6 = -2\pi \int_{\ell_o}^{x} p_b' r_b \tan\phi \, dx' \quad , \tag{16}$$

$$F_7 = -2\pi \int_{\ell_o}^{x} r_b \tau_b \, dx' \quad , \tag{17}$$

and

$$F_8 = -2\pi r_w \int_{o}^{x} \tau_w \, dx' \quad . \tag{18}$$

The quantity p_V is the viscous pressure that occurs in the fluid between the body and tunnel wall at location x , and p_b' is the "displaced-body" pressure, i.e., it is a perturbed p_b due to the added acceleration of the flow caused by the body boundary-layer development. It may be calculated using potential flow methods, but with the body radius re-defined by $r_b' = r_b + \delta_b^*$, where δ_b^* is the body boundary-layer displacement thickness. In Eq.'s (17) and (18), τ_b and τ_w are the wall shear stresses that occur on the body and tunnel wall, respectively. It is noted that F_7 does not contain a $\cos\phi$ term because F_7, by assumption, is the x-component of the force due to body wall shear stress. Equation (13) can be readily solved for p_V to obtain an analogous form of Eq. (11) for viscous flow.

Pressure Coefficient Correction

To obtain a viscous flow correction for the in-tunnel, inviscid pressure coefficient, Cp_I , we form the difference

$$p_V - p_I = \rho \, U_\infty^2 \, \frac{A_o^2}{A^2} + \frac{2\pi}{A} \left\{ \int_{\ell_o}^{x} p_b \, r_b \, \tan\phi \, dx' - \int_{\ell_o}^{x} p_b' \, r_b \, \tan\phi \, dx' \right.$$

$$\left. - \int_{\ell_o}^{x} r_b \, \tau_b \, dx' - r_w \int_{o}^{x} \tau_w \, dx' - \rho \int_{r_b}^{r_w} u^2 \, rdr \right\} \quad , \quad (19)$$

where the change of variable $x = \bar{x} + \ell_o$ was made in Eq. (11).

A pressure coefficient correction term may be defined by:

$$\Delta Cp = Cp_V - Cp_I \quad , \tag{20}$$

where

$$Cp_V = \frac{p_V - p_o}{\frac{1}{2} \, \rho \, U_\infty^2} \quad , \tag{21}$$

and

$$Cp_I = \frac{p_I - p_o}{\frac{1}{2} \, \rho \, U_\infty^2} \quad , \tag{22}$$

such that

$$\Delta Cp = \frac{p_V - p_I}{\frac{1}{2} \, \rho \, U_\infty^2} \quad . \tag{23}$$

It is convenient to express ΔCp as the sum of individual terms, i.e.,

$$\Delta Cp = \sum_{i=1}^{4} \Delta Cp_i \quad , \tag{24}$$

where

$$\Delta Cp_1 = 2 \frac{A_o^2}{A^2} - \frac{4\pi}{A U_\infty^2} \int_{r_b}^{r_w} u^2 \, r dr \qquad , \qquad (25)$$

$$\Delta Cp_2 = - \frac{4\pi}{A \rho U_\infty^2} \int_{\ell_o}^{x} r_b \tau_b \, dx' \qquad ; \qquad (26)$$

$$\Delta Cp_3 = - \frac{4\pi r_w}{A \rho U_\infty^2} \int_{o}^{x} \tau_w \, dx' \qquad , \qquad (27)$$

and

$$\Delta Cp_4 = \frac{4\pi}{A \rho U_\infty^2} \left\{ \int_{\ell_o}^{x} p_b r_b \tan\phi \, dx' - \int_{\ell_o}^{x} p_b' r_b \tan\phi \, dx' \right\} . \qquad (28)$$

Under the assumption that a turbulent boundary layer originates at $x = 0$, and that $(\ell_o + L) \lesssim 10 \, r_w$, then the wall shear stress, τ_w , can be calculated from flat-plate expressions [6, 7]. After making the substitution [6]

$$\tau_w = 0.0225 \, \rho \, U_\infty^2 \left[\frac{\nu}{U_\infty \delta_w} \right]^{1/4} \qquad (29)$$

into Eq. (27), where the boundary-layer thickness is given by

$$\delta_w = 0.37 \, x \left[\frac{U_\infty x}{\nu} \right]^{-1/5} \qquad , \qquad (30)$$

we can evaluate the integral of Eq. (27) in closed form. Thus, we find that

$$\Delta Cp_3 = -r_w \frac{0.144 \, \pi}{A} \left(\frac{\nu}{U_\infty} \right)^{1/5} x^{4/5} \qquad , \qquad (31)$$

where ν is the kinematic viscosity, and $A = A_o$ for $x \leq \ell_o$. For arbitrarily-shaped bodies, the integrals of Eq.'s (26) and (28) must be evaluated numerically.

The integral of Eq. (25), however, may be evaluated in closed form if we make certain assumptions regarding the velocity profile $u(r)$. Clearly,

$$I_i \equiv \int_{r_b}^{r_w} u^2 \, rdr = \int_{r_b}^{r_b+\delta_i} u_i^2 \, rdr + u_V^2 \int_{r_b+\delta_i}^{r_w-\delta_w} rdr + \int_{r_w-\delta_w}^{r_w} u_w^2 \, rdr \quad , (32)$$

where subscript i equals 1 for laminar-body flow and is equal to 2 for turbulent-body flow. The boundary-layer velocity profile, u_w, at the tunnel wall is (as above) assumed turbulent, i.e., [6],

$$u_w = u_V \left(\frac{r_w - r}{\delta_w} \right)^{1/7} \quad . \tag{33}$$

On the turbulent-flow body, we have:

$$u_2 = u_V \left(\frac{r - r_b}{\delta_2} \right)^{1/7} \quad , \tag{34}$$

where δ_2 is of the same analytical form as Eq. (30), but with x being replaced by the arc length coordinate, s. For the case of a laminar-flow body we assume a sine function velocity profile, which according to Schlichting [6], very accurately approximates the exact Blasius profile. Thus, we assume

$$u_1 = u_V \sin \left(\frac{\pi (r - r_b)}{2 \, \delta_1} \right) \quad , \tag{35}$$

with

$$\delta_1 = 4.7953 \, (\nu s/U_\infty)^{1/2} \quad . \tag{36}$$

With these assumed velocity profiles, Eq. (32) can be integrated. Without showing the details, we find:

$$I_1 = u_V^2 \left\{ \left(\frac{4 - \pi^2}{4\pi^2} \right) \delta_1^2 - \frac{r_b \delta_1}{2} + \frac{\delta_w^2}{16} - \frac{2}{9} r_w \delta_w + \left(\frac{r_w^2 - r_b^2}{2} \right) \right\} \quad (37)$$

for laminar flow on the body, and

$$I_2 = u_V^2 \left\{ - \frac{\delta_2^2}{16} - \frac{2}{9} r_b \delta_2 + \frac{\delta_w^2}{16} - \frac{2}{9} r_w \delta_w + \left(\frac{r_w^2 - r_b^2}{2} \right) \right\} \quad (38)$$

for turbulent flow on the body.

We now eliminate u_V^2 from I_i ; thus, Eq. (12) must be integrated. Again, we write

$$B_i \equiv \int_{r_b}^{r_w} u \; r dr = \int_{r_b}^{r_b + \delta_i} u_i \; r dr + u_V \int_{r_b + \delta_i}^{r_w - \delta_w} r dr + \int_{r_w - \delta_w}^{r_w} u_w \; r dr \quad , \quad (39)$$

finding

$$B_1 = u_V \left\{ \left(\frac{8 - \pi^2}{2\pi^2} \right) \delta_1^2 + \left(\frac{2 - \pi}{\pi} \right) r_b \delta_1 + \frac{\delta_w^2}{30} - \frac{r_w \delta_w}{8} + \left(\frac{r_w^2 - r_b^2}{2} \right) \right\} (40)$$

and

$$B_2 = u_V \left\{ \left(\frac{\delta_w^2 - \delta_2^2}{30} \right) - \left(\frac{r_w \delta_w + r_b \delta_b}{8} \right) + \left(\frac{r_w^2 + r_b^2}{2} \right) \right\} \quad . \quad (41)$$

Because $B_i = A_o U_\infty/2\pi$ we obtain for $i = 1$ (laminar flow):

$$u_V = A_o U_\infty \left\{ A - \left(\frac{8 - \pi^2}{\pi}\right) \delta_1^2 + 2(2-\pi) r_b \delta_1 - \frac{\pi r_w \delta_w}{4} + \frac{\pi}{15} \delta_w^2 \right\}^{-1}, \quad (42)$$

and for $i = 2$ (turbulent flow):

$$u_V = A_o U_\infty \left\{ A - \frac{\pi}{4} (r_b \delta_2 + r_w \delta_w) + \frac{\pi}{15} (\delta_w^2 - \delta_2^2) \right\}^{-1} . \quad (43)$$

The first term of ΔC_p may be expressed in the form $\Delta C_{p_1} = \Delta C_{p_{1i}}$ ($i=1$ or 2). For laminar flow on the body, we find:

$$\Delta C_{p_{11}} = 2\frac{A_o^2}{A^2} - \frac{2A_o^2 \left\{ A + \left(\frac{4-\pi^2}{2\pi}\right)\delta_1^2 - \pi r_b \delta_1 - \frac{4\pi r_w \delta_w}{9} + \frac{\pi \delta_w^2}{8} \right\}}{A \left\{ A - \left[\frac{8-\pi^2}{\pi}\right]\delta_1^2 + 2(2-\pi) r_b \delta_1 - \frac{\pi r_w \delta_w}{4} + \frac{\pi}{15} \delta_w^2 \right\}^2} , \quad (44)$$

and for turbulent flow on the body, we find:

$$\Delta C_{p_{12}} = 2\frac{A_o^2}{A^2} - \frac{2A_o^2 \left\{ A - \frac{4\pi}{9} (r_w \delta_w + r_b \delta_2) + \frac{\pi}{8} (\delta_w^2 - \delta_2^2) \right\}}{A \left\{ A - \frac{\pi}{4} (r_w \delta_w + r_b \delta_2) + \frac{\pi}{15} (\delta_w^2 - \delta_2^2) \right\}^2} . \quad (45)$$

If the boundary layers are thin, one may of course neglect the higher order terms in δ_w and δ_i .

APPLICATION OF THE THEORY

Body Shape

Based on the above analysis, computations have been performed for a large, streamlined body designed to operate in the Garfield Thomas 1.22-m. diameter Water Tunnel [8]. This body was referred to in the INTRODUCTION and is described mathematically by:

$$\hat{y} = \sqrt{\hat{x}(2-\hat{x})} - K_n \frac{C_o \hat{x}}{2a^2} \exp\left\{-\frac{\hat{x}^2}{2a^2} - k\,K_n\right\} + \hat{x}^2\,\epsilon_L \quad, \qquad (46)$$

where $\hat{x} = \hat{x}/\ell_n$, ℓ_n = nose length, $\hat{y} = r_b/D_{max}/2$, D_{max} = maximum diameter of the body, $K_n = \ell_n/D_{max}$, and a, C_o, and k are numerical constants. The parameter

$$\epsilon_L = \frac{K_n\,C_o}{2a^2} \exp\left\{-\frac{1}{2a^2} - k\,K_n\right\} \qquad . \qquad (47)$$

The tailcone is formed by an 18° arc of radius

$$R_L = \frac{2.5\,D_{max}}{2 \sin 18^o} \qquad . \qquad (48)$$

An inflection curve is then faired between the end of the arc (at $\phi = 90-18 = 72^o$) and a 4-inch diameter disk whose center is coincident with the axis of symmetry. This body shape was shown in Figure 1 for $a = 0.3$, $C_o = 0.0303$, and, $k = 0.45227$. The total length, L , is 3.05-m., and D_{max} is 32.39 cm.

Experimental Pressure Distributions

The experimental body was manufactured by building up multiple layers of fiberglass cloth and resin. A precision template was used to screed the body to final shape before the last coating of resin fully hardened. Figure 3 shows

a photograph of the completed body and sting mount used to hold it in the 1.22-m. diameter test section. A total of 94 pressure taps were located in the surface of the body. These pressure orifices were 0.79-mm. in diameter. Each body tap was connected to a flexible plastic tube which passed through the inside of the body, through the sting, and out of the tunnel. The 94 tubes then connected to two 48-channel Scanivalves and a single Bell and Howell calibrated pressure transducer. Before all runs, the tubes were bled to remove air pockets. Figure 4 shows a schematic of the experimental arrangement and the equations used in data reduction to obtain Cp_E.

As indicated in Figures 2(c) and 4 the reference velocity in the measurements, u_m, was obtained with a pitot probe placed relatively close to the body and tunnel wall. Consequently, u_m may not be interpreted as the U_∞ used in the theoretical analysis. The velocity u_m differs from U_∞ because of both potential effects induced by the body and viscous effects created by tunnel wall boundary-layer growth.

Detailed measurements of the turbulent boundary layer growth on the wall of the Garfield Thomas Water Tunnel were performed and reported by Ross, et al [7]. They concluded that an effective origin for the start of boundary layer growth is 1.5 r_w upstream from the geometric beginning of the test section. That is, one may assume that the cylindrical test section can be ficticiously extended upstream into the settling section a distance 1.5 r_w and refer to this point as the entrance of the test section, Figure 2(c). Thus, we can assume $\ell_o = 1.5 r_w + d_o$, where d_o is the distance from the nose of the body to the actual beginning of the cylindrical test section (d_o = 54.6 cm. in this arrangement).

In order to compare our experimental pressure distributions with theoretically predicted ones, it is apparent that Cp_E (referenced to u_m) must be

corrected in order to account for the differences between u_m and U_∞. We do this in two steps.

We first correct Cp_E for the tunnel wall boundary-layer displacement thickness at the position of the pitot probe. This thickness varies from 2.02-mm. at 15.24 m./sec. to 2.42-mm. at 6.09m./sec. (the range of velocities considered in this investigation). The pitot probe was 4-inches from the wall and thus was out of the boundary layer. The effective area of the tunnel at the position of the pitot probe is:

$$A_e = A_o - 2\pi \ r_w \ \delta_w^* + \pi \ \delta_w^{\ 2}$$

$$\simeq A_o - 2\pi \ r_w \ \delta_w^* \quad . \tag{49}$$

From the continuity equation [Eq. (12)], we can write

$$\left(\frac{u_m}{U_\infty} \right)_V = \frac{A_o}{A_e} \quad , \tag{50}$$

which represents the increase in u_m relative to U_∞ due to boundary-layer growth. The experimental pressure coefficient corrected to U_∞ by viscous considerations only is thus:

$$Cp_E^V = 1 - \left(\frac{u_E}{u_m} \right)^2 \left(\frac{u_m}{U_\infty} \right)_V^2$$

$$= 1 - (1 - Cp_E) \left(\frac{A_o}{A_e} \right)^2 \quad . \tag{51}$$

We know (because of the close proximity of the pitot probe to the body) that u_m may also be influenced by the potential effects of the body. In order to correct for this, a potential flow solution, such as that obtained

from the Douglas-Neumann code is required. We calculate the velocity ratio $u_{rp} = U_\infty/u_m$ at the pitot probe location. Then,

$$Cp_E^{cor.} = 1 - (1 - Cp_E^V)/u_{rp}^2 \qquad (52)$$

is the final correction of Cp_E. Furthermore it makes no difference which correction is applied first, i.e.,

let

$$Cp_E^I = 1 - (1 - Cp_E)/u_{rp}^2 \qquad ,$$

then

$$Cp_E^{cor.} = 1 - (1 - Cp_E^I)\left(\frac{A_o}{A_e}\right)^2 \qquad ,$$

$$= 1 - \left(\frac{A_o}{A_e\, u_{rp}}\right)^2 + Cp_E\left(\frac{A_o}{A_e\, u_{rp}}\right)^2 \qquad . \qquad (53)$$

It is easily verified that Eq. (52) also reduces to Eq. (53). For the experimental arrangement used here, we found $u_{rp} = 0.9976$, and that A_o/A_e ranges from 1.013 to 1.016.

The experimental pressure distributions shown in Figure 1 have been corrected according to the above discussion.

Results

The generality of the above analysis allows both laminar and turbulent-body flow. As part of the experimental program, we therefore measured the laminar-to-turbulent transition points at the four tunnel velocities in which pressure distributions were measured. A wedge-shaped hot-film probe and anemometer system were used in these measurements. TABLE I summarizes the

transition location results. For those body coordinates forward of s_t (transition arc length), the laminar form of the pressure coefficient correction analysis is used [Eq. (44)]. And, τ_b in Eq. (26) is calculated according to the formula

$$\tau_b = 0.332 \; \rho \; \nu \; U_\infty \; (U_\infty/\nu \; s)^{1/2} \tag{54}$$

in this laminar-flow regime. For $s > s_t$, τ_b is calculated according to Eq. (29) with the appropriate change from x to s variable. The integral of Eq. (26) is evaluated using Simpson's Rule of numerical integration.

The integrals of Eq. (28) are also evaluated using Simpson's Rule. Both p_b and p_b' are determined from the body-in-a cylindrical duct Douglas-Neumann solution. In this numerical example we calculated δ_b^* (needed to obtain p_b') using an axisymmetric, implicit finite-difference solution of the boundary layer equations of motion.

Because of the thicker boundary layers, ΔCp is largest at the lower velocities. Thus, at 6.09 m./sec. a few typical values of ΔCp_i ($i=1,2,3,4$) are presented in TABLE II from which an assessment of each ΔCp_i's contribution to the total ΔCp can be made. Clearly, ΔCp_3 contributes the greatest to ΔCp, but ΔCp_1 and ΔCp_2 are also significant contributors. On the other hand, ΔCp_4 is approximately an order of magnitude lower than ΔCp_2 ($\Delta Cp_2 < \Delta Cp_1 < \Delta Cp_3$) for those locations on the body where the flow is turbulent. Obviously, ΔCp_4 is the most tedious to calculate, so it may be conveniently justified to neglect it entirely from the computations. For those conditions in which the computations are compared to experimental data, this deletion has been made. It is further noted, that if body-flow is entirely laminar, ΔCp_2 may also be neglected; although, we have retained

it for all of the computations in this example because there is only a small regime of laminar flow on the body.

Figures 5 through 8 summarize the comparisons of potential flow, corrected potential flow, and experimental pressure distributions for our given body operating at 6.09 through 15.24 m./sec. test-section velocities. At all speeds the horizontal buoyancy correction theory agrees well with the experimental data, particularly for those body positions forward of Cp_{min}. Aft of Cp_{min}, there is a region of strong interaction where coupling between the boundary-layer flow and the potential outer flow becomes important. The theory presented here is not applicable to this region.

CONCLUSIONS

The analysis presented here is applicable to many practical problems involving the flow about bodies of revolution within cylindrical ducts, such as wind or water tunnel test sections. In particular, this analysis allows one to correct an inviscid, in-duct body pressure distribution for the effects of horizontal buoyancy. The derived expressions are relatively simple; thus, computations are performed using very simple Fortran or desk-top calculator programs. Based on the experimental observations of, and on the computations performed for a particular body that operates in a given water tunnel test section, horizontal buoyancy effects were shown to be important and should not be neglected if precise pressure coefficient values are required. We have demonstrated that the theory adequately predicts the observed effects, except in the afterbody region where strong interaction effects dominate.

REFERENCES

1. Hess, J. L. and Martin, Jr., R. P., "Improved Solution for Potential Flow About Arbitrary Axisymmetric Bodies by the Use of a Higher Order Surface Source Method: Part I. Theory and Results," NASA CR 134694, MDC J6627-01, July 1974.

2. Friedman, D. M., "Improved Solution for Potential Flow About Arbitrary Axisymmetric Bodies by the Use of a Higher-Order Surface Source Method: Part II. User's Manual for Computer Program," NASA CR 134695, MDC J6627-02, July 1974.

3. Goodman, T. R., "Aerodynamic Characteristics of a Slender Body Traveling in a Tube," AIAA Journal, Vol. 9, April 1971, pp. 712-717.

4. Landweber, L., "Axisymmetric Potential Flow in a Circular Tube," Journal of Hydronautics, Vol. 8, Oct. 1974, pp. 137-145.

5. Varsamov, K. and Haimov, A., "Axisymmetric Potential Flow in Ducts," Journal of Hydronautics, Vol. 12, April 1978, pp. 78-80.

6. Schlichting, H., Boundary-Layer Theory, 6th ed., McGraw-Hill Book Co., New York, 1968.

7. Ross, D. and McGinley, J. H., "Flow in Closed-Jet Working Sections," Ordnance Research Laboratory External Report NOrd 7958-283, Feb. 5, 1954, The Pennsylvania State University, Applied Research Laboratory, State College, PA 16801.

8. Lehman, A. F., "The Garfield Thomas Water Tunnel," Ordnance Research Laboratory External Report NOrd 16597-56, Sept. 30, 1959, The Pennsylvania State University, Applied Research Laboratory, State College, PA 16801.

Table I The experimentally determined transition points on the body used in the pressure distribution measurements.

Tunnel Velocity U_∞ (m./sec.)	Body-Length Reynolds No. $Re_L = U_\infty L/\nu$	Transition Point s_t/L	Transition Reynolds No. $Re_L(s_t/L)$
6.09	1.88×10^7	0.150	2.82×10^6
9.14	2.83×10^7	0.116	3.28×10^6
12.19	3.76×10^7	0.100	3.76×10^6
15.24	4.72×10^7	0.083	3.93×10^6

Table II Typical values for ΔCp_i ($i = 1, 2, 3, 4$) at 6.09 m./sec., the inviscid pressure coefficient, and the corrected inviscid pressure coefficient for horizontal buoyance effects.

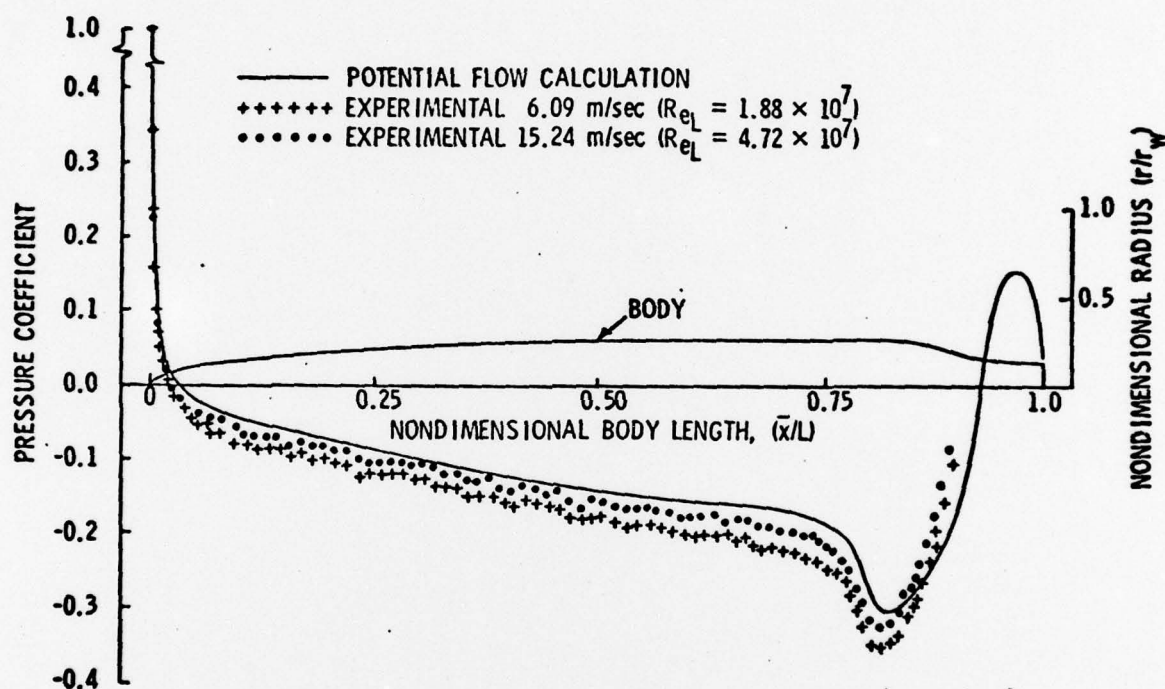| Body Coordinate $\bar{x}/L = (x-\ell_o)/L$	ΔCp_1	ΔCp_2	ΔCp_3	ΔCp_4	$\Delta Cp = \sum\limits_{i=1}^{4} \Delta Cp_i$	Cp_I	Cp_V
0.002	-0.0038	0.000	-0.0139	0.00009	-0.0177	0.433	0.415
0.075	-0.0046	-0.00003	-0.0158	0.00047	-0.0199	-0.036	-0.056
0.253	-0.0065	-0.0006	-0.0202	0.00061	-0.0267	-0.087	-0.113
0.497	-0.0091	-0.0020	-0.0261	0.00069	-0.0366	-0.139	-0.176
0.667	-0.0108	-0.0031	-0.0300	0.00071	-0.0432	-0.161	-0.204

Figure 1 The pressure distributions on a large axisymmetric body
(L = 3.05-m.) operating in a cylindrical test section
(r_w = 1.22-m.)

POTENTIAL FLOW - C_{P_I}

CORRECTION OF POT. FLOW FOR VISCOUS EFFECTS - $C_{P_V} = C_{P_I} + \Delta C_P$

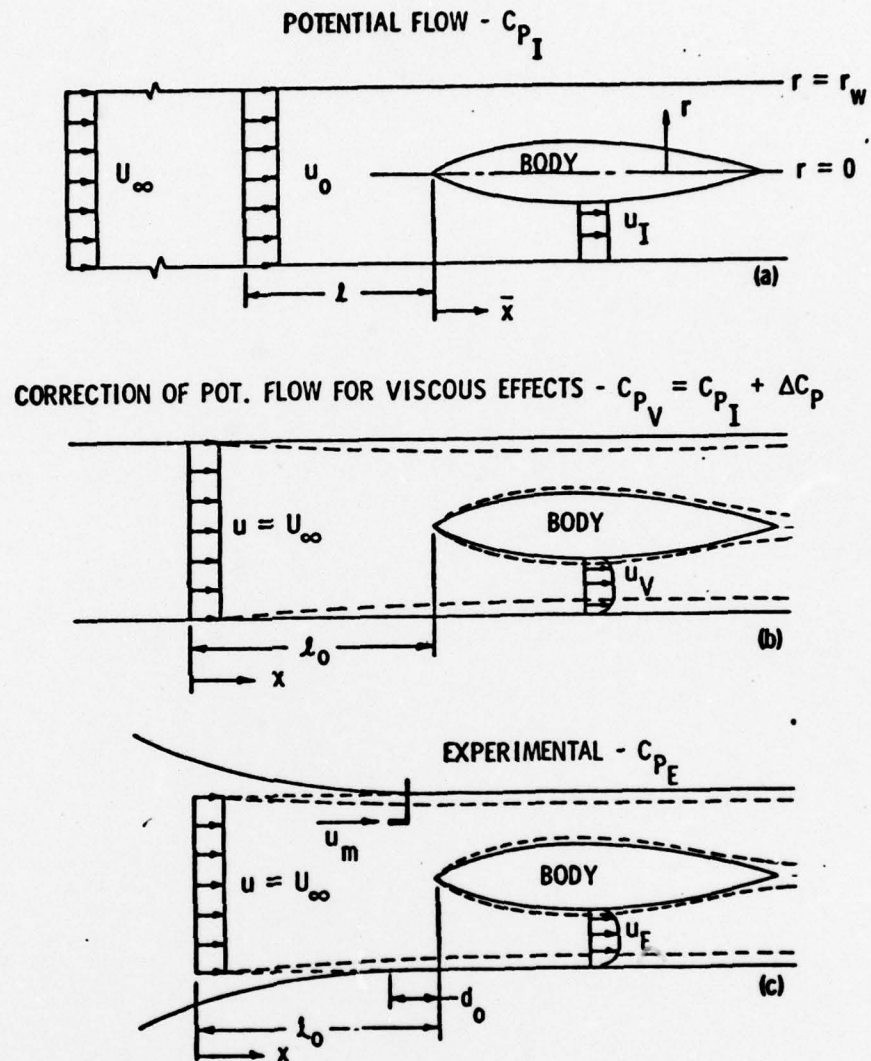
EXPERIMENTAL - C_{P_E}

Figure 2 (a) Potential flow over a body in an infinitely long cylindrical duct, (b) a schematic description of boundary layer buildup on the body and duct wall depicting that u_V is different from u_I, and (c) a schematic description of the flow over a body in an experimental situation.
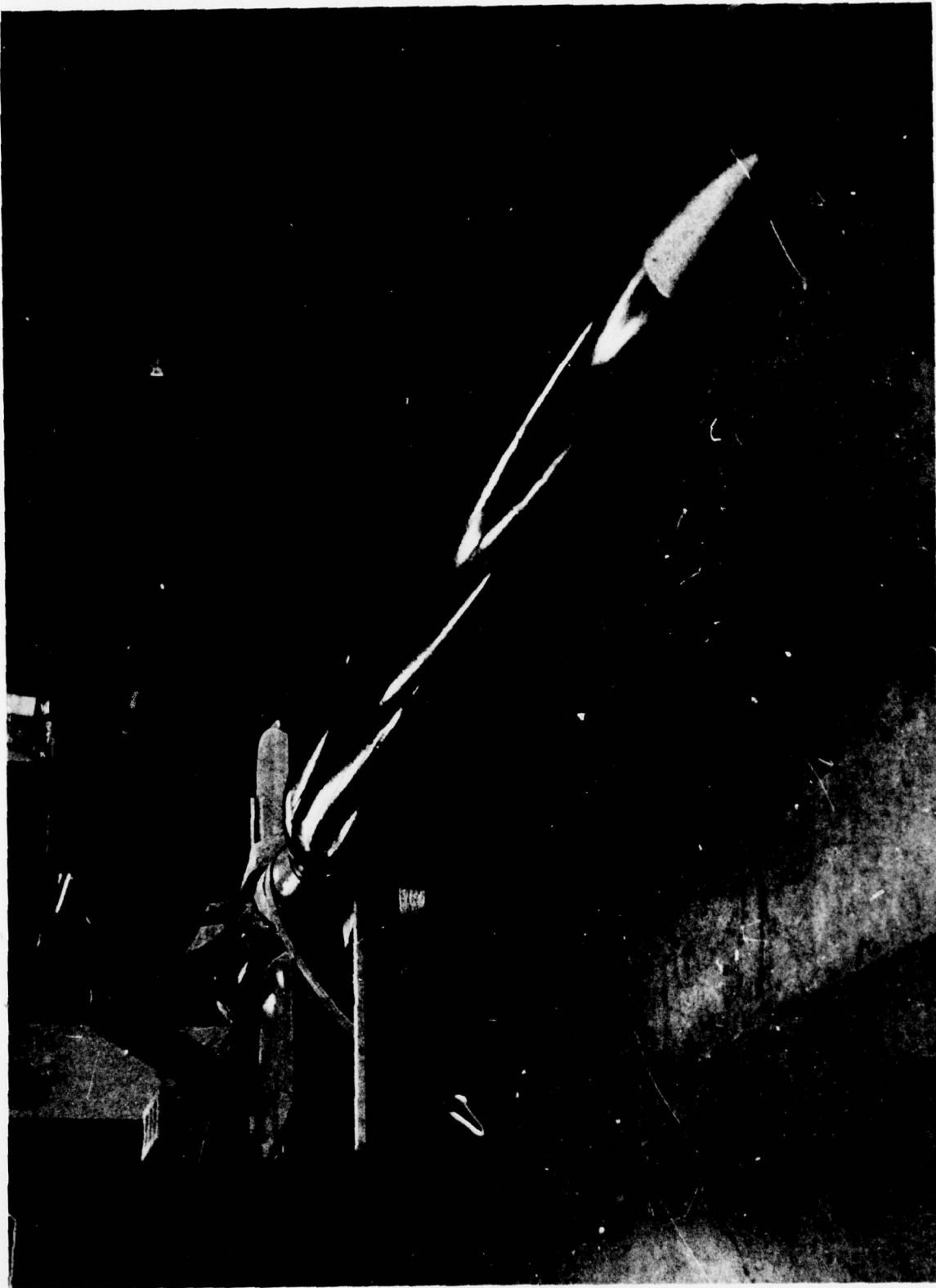
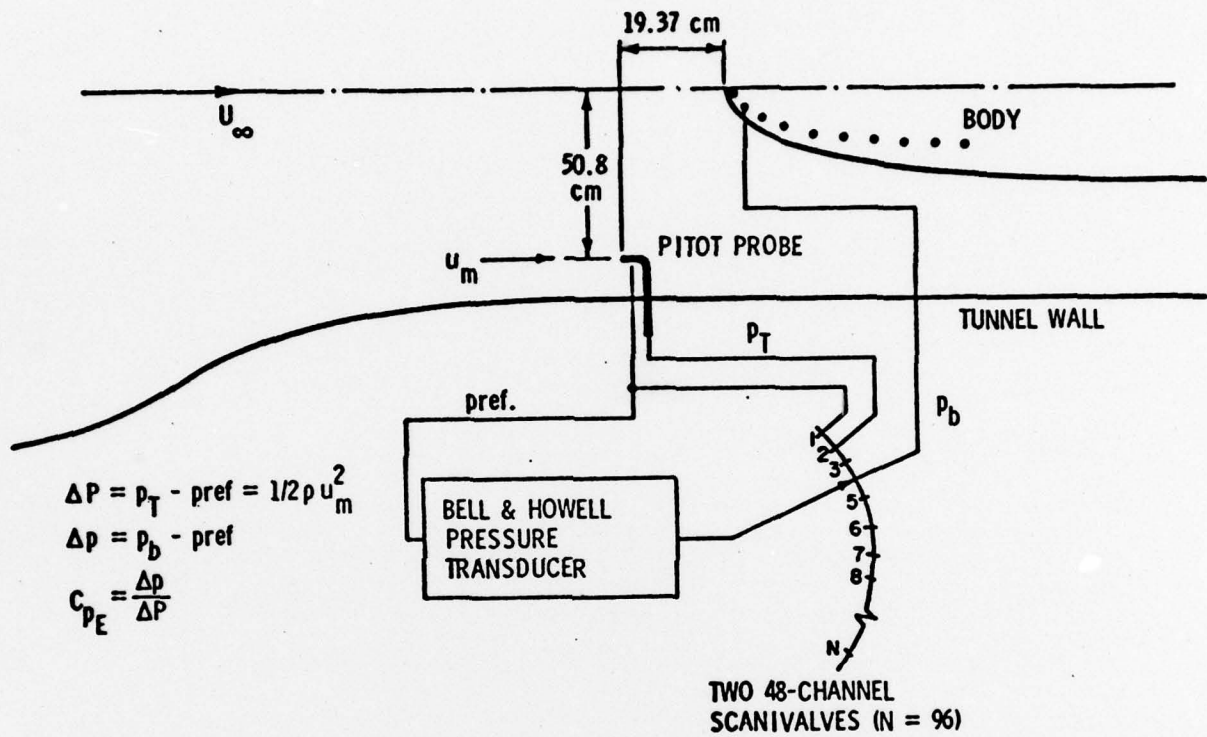Figure 3 The body used in the experimental portion of this investigation.

Figure 4 A schematic of the data acquisition and reduction requirements
used to obtain the experimental pressure distributions.
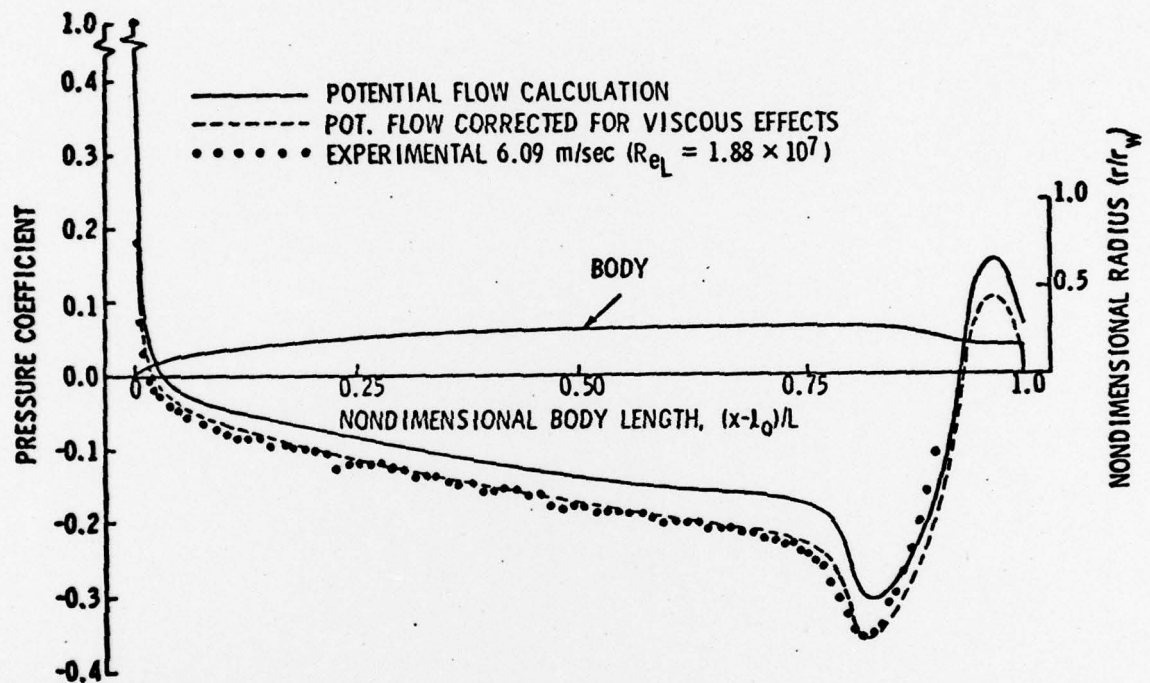
Figure 5   A comparison of the in-tunnel potential flow and corrected
            potential flow pressure distributions with one determined
            experimentally at 6.09 m./sec. in the 1.22-m. diameter
            water tunnel.

Figure 6 A comparison of the in-tunnel potential flow and corrected potential flow pressure distributions with one determined experimentally at 9.14 m./sec. in the 1.22-m. diameter water tunnel.

Figure 7 A comparison of the in-tunnel potential flow and corrected potential flow pressure distributions with one determined experimentally at 12.19 m./sec. in the 1.22-m. diameter water tunnel.
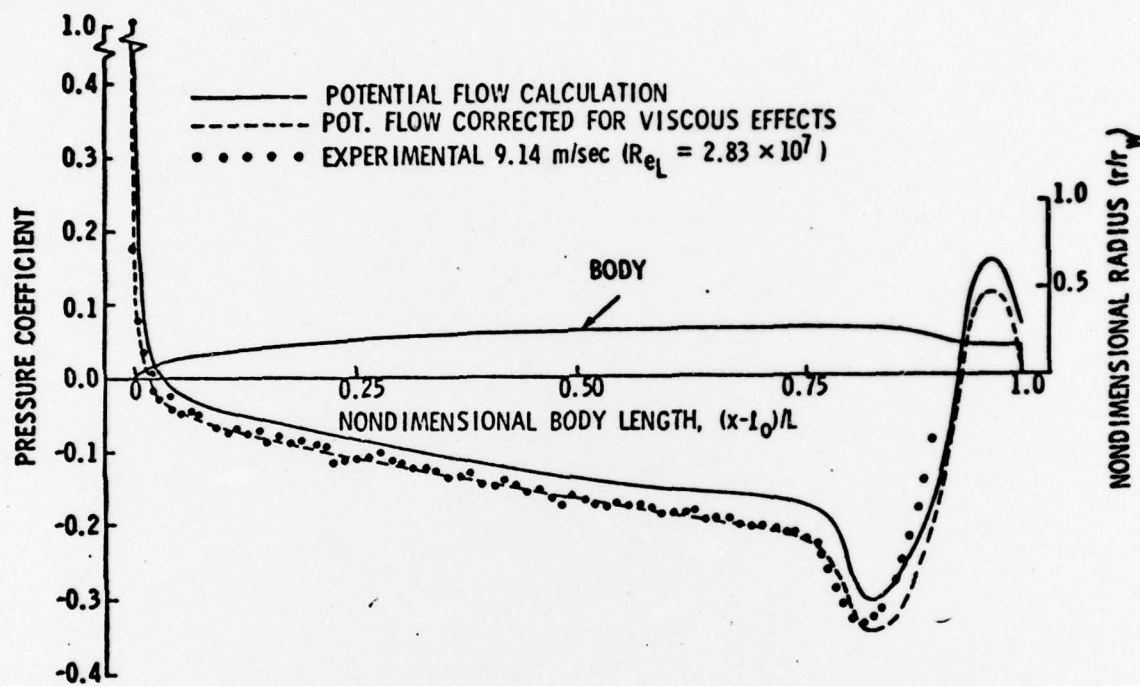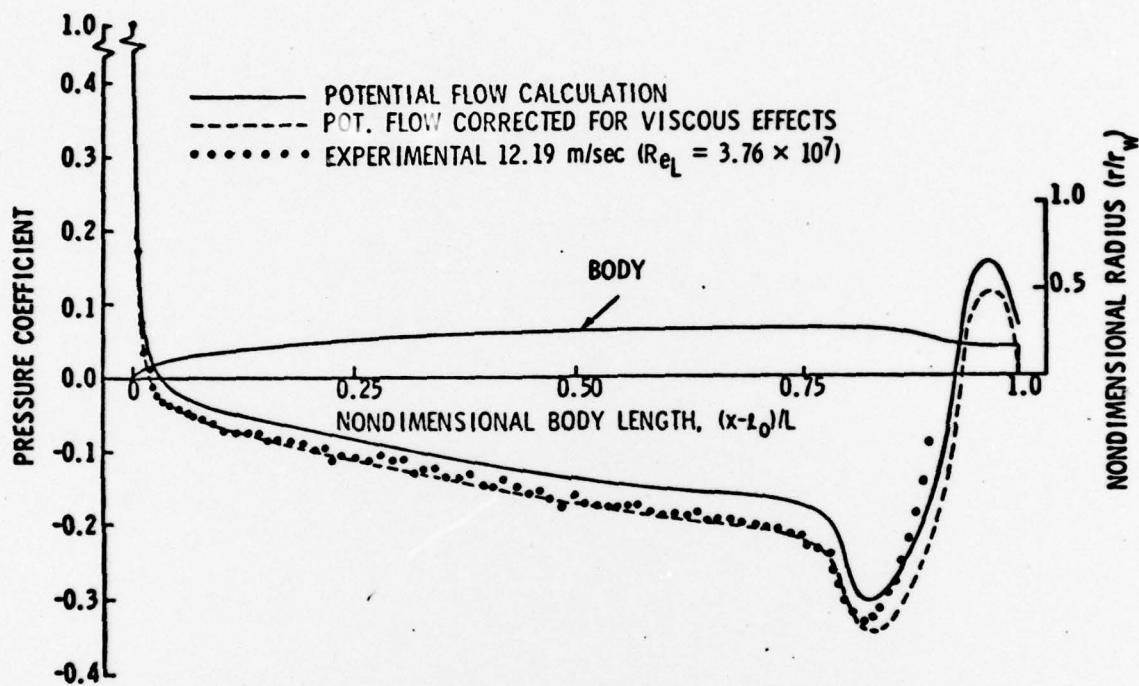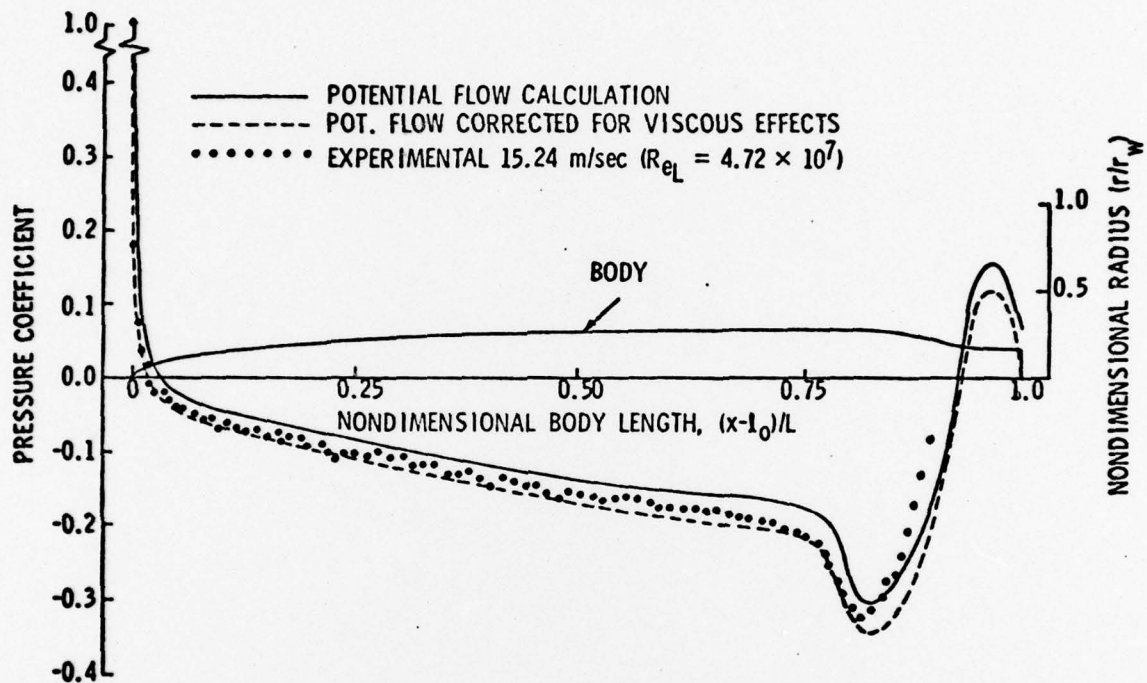
Figure 8   A comparison of the in-tunnel potential flow and corrected
potential flow pressure distributions with one determined
experimentally at 15.24 m./sec. in the 1.22-m. diameter
water tunnel.

Commander
Naval Sea Systems Command
Department of the Navy
Washington, DC 20362
Attn: Library
       Code NSEA-09G32
(Copies No. 1 and 2)

Naval Sea Systems Command
Attn: A. V. Bress
       Code NSEA-03
(Copy No. 3)

Naval Sea Systems Command
Attn: C. G. McGuigan
       Code NSEA-03133
(Copy No. 4)

Naval Sea Systems Command
Attn: L. Benen
       Code NSEA-0322
(Copy No. 5)

Naval Sea Systems Command
Attn: E. J. McKinney
       Code NSEA-0342
(Copy No. 6)

Naval Sea Systems Command
Attn: E. G. Liszka
       Code NSEA-0342
(Copy No. 7)

Naval Sea Systems Command
Attn: G. Sorkin
       Code NSEA-035
(Copy No. 8)

Naval Sea Systems Command
Attn: T. E. Peirce
       Code NSEA-0351
(Copy No. 9)

Naval Sea Systems Command
Attn: J. G. Juergens
       Code NSEA-037
(Copy No. 10)

Naval Sea Systems Command
Attn: H. C. Claybourne
       Code NSEA-0371
(Copy No. 11)

Naval Sea Systems Command
Attn: A. R. Paladino
       Code NSEA-0372
(Copy No. 12)

Naval Sea Systems Command
Attn: D. Creed
       Code NSEA-03132A
(Copy No. 13)

Commander
Naval Ship Engineering Center
Department of the Navy
Washington, DC 20360
Attn: W. L. Louis
       Code NSEC-6136B
(Copy No. 14)

Naval Ship Engineering Center
Attn: R. J. Cauley
       Code NSEC-6140B
(Copy No. 15)

Naval Ship Engineering Center
Attn: F. Welling
       Code NSEC-6144
(Copy No. 16)

Naval Ship Engineering Center
Attn: R. M. Petros
       Code NSEC-6148
(Copy No. 17)

Naval Ship Engineering Center
Attn: D. Burke
       Code NSEC-6113C1
(Copy No. 18)

Commanding Officer
Naval Underwater Systems Center
Newport, RI 02840
Attn: Technical Director
       Code SB3
(Copy No. 19)

Naval Underwater Systems Center
Attn: D. Goodrich
       Code SB323
(Copy No. 20)

Naval Underwater Systems Center
Attn: R. Nadolink
          Code SB323
(Copy No. 21)

Naval Underwater Systems Center
Attn: R. Trainor
          Code SB323
(Copy No. 22)

Naval Underwater Systems Center
Attn: F. White
          Code SB332
(Copy No. 23)

Naval Underwater Systems Center
Attn: Library
          Code LA15
(Copy No. 24)

Commanding Officer
Naval Ocean Systems Center
San Diego, CA 92152
Attn: J. W. Hoyt
          Code 2501
(Copy No. 25)

Naval Ocean Systems Center
Attn: D. Nelson
          Code 2542
(Copy No. 26)

Naval Ocean Systems Center
Attn: A. G. Fabula
          Code 5311
(Copy No. 27)

Naval Ocean Systems Center
Attn: G. Donohue
(Copy No. 28)

Naval Ocean Systems Center
Attn: M. Reischman
(Copy No. 29)

Commanding Officer and Director
David W. Taylor Naval Ship Research
and Development Center
Department of the Navy
Bethesda, MD 20084
Attn: W. E. Cummins
          Code 15
(Copy No. 30)

David W. Taylor Naval Ship Research
and Development Center
Attn: S. F. Crump
          Code 1505
(Copy No. 31

David W. Taylor Naval Ship Research
and Development Center
Attn: W. B. Morgan
          Code 154
(Copy No. 32)

David W. Taylor Naval Ship Research
and Development Center
Attn: R. Cumming
          Code 1544
(Copy No. 33)

David W. Taylor Naval Ship Research
and Development Center
Attn: J. McCarthy
          Code 1552
(Copy No. 34)

David W. Taylor Naval Ship Research
and Development Center
Attn: M. Sevik
          Code 19
(Copy No. 35)

Commanding Officer and Director
David W. Taylor Naval Ship Research
and Development Center
Department of the Navy
Annapolis Laboratory
Annapolis, MD 21402
Attn: J. G. Stricker
          Code 2721
(Copy No. 36)

Commander
Naval Surface Weapon Center
Silver Spring, MD 20910
Attn: Library
(Copy No. 37)

Office of Naval Research
Department of the Navy
800 N. Quincy Street
Arlington, VA 22217
(Copy No. 38)

Defense Documentation Center
5010 Duke Street
Cameron Station
Alexandria, VA 22314
(Copies No. 39 to and
including 50)

National Bureau of Standards
Aerodynamics Section
Washington, DC 20234
Attn: P. S. Klebanoff
(Copy No. 51)

Rand Corporation
1700 Main Street
Santa Monica, CA 90406
Attn: R. King
(Copy No. 52)

Rand Corporation
Attn: C. Gazley
(Copy No. 53)

Defense Advanced Research Projects Agency
1400 Wilson Boulevard
Arlington, VA 22209
Attn: P. Selwyn, TTO
(Copy No. 54)

Naval Research Laboratory
Washington, DC 20390
Attn: R. J. Hansen
(Copy No. 55)

Dr. J. L. Lumley
Sibley School of Mechanical and
Aeronautical Engineering
Upson and Graumman Halls
Cornell University
Ithaca, NY 14850
(Copy No. 56)

Applied Research Laboratory
The Pennsylvania State University
Post Office Box 30
State College, PA 16801
Attn: B. R. Parkin
(Copy No. 57)

Applied Research Laboratory
Attn: G. C. Lauchle
(Copy No. 58)

Applied Research Laboratoty
Attn: R. F. Davis
(Copy No. 59)

Applied Research Laboratory
Garfield Thomas Water Tunnel Library
(Copy No. 60)

David W. Taylor Naval Ship Research
and Development Center
Attn: W. K. Blake
      Code 1900
(Copy No. 61)

Naval Surface Weapon Center
Attn: G. Gaunaurd
      Code K-31
(Copy No. 62)